Single EMG Sensor-Driven Robotic Glove Control for Reliable Augmentation of Power Grasping

Sangheui Cheon, *Graduate Student Member, IEEE*, Daekyum Kim, *Member, IEEE*, Sudeok Kim, Brian Byunghyun Kang, *Member, IEEE*, Jongeun Lee, *Graduate Student Member, IEEE*, HyunSik Gong, Sungho Jo, *Senior Member, IEEE*, Kyu-Jin Cho, *Member, IEEE*, and Jooeun Ahn

***Abstract*—The practical operation of wearable robots requires intuitive, compact, yet reliable control interfaces. However, current myoelectric interfaces based on surface electromyography (EMG) often fail to achieve these requirements by demanding multiple sensors and exhibiting unreliable performance under limb posture changes. In this study, we show that a myoelectric interface on the *musculotendinous junctions* (MTJs) of the flexor digitorum superficialis (FDS) enables reliable control of a robotic glove with a single EMG sensor by identifying power grasp intentions. We found that the myoelectric signals from the MTJs of the FDS show significantly increased amplitudes exclusively when a power grasp is performed, regardless of the arm posture. We systematically verified that, in identifying power grasp intentions, the proposed single-sensor myoelectric interface even outperforms a five-sensor myoelectric interface around the proximal forearm. By exploiting the unique biological feature of the MTJs, we devised two myoelectric control methods for a robotic glove—Dual-threshold control and Morse-code control—and further showed their performances in practical operations. Dual-threshold control enables direct co-operation between the user and the robotic glove, and Morse-code control provides various command options for the user.**

***Index Terms*—Wearable robots, exoskeletons, robotic glove, exo-glove, electromyography, musculotendinous junctions.**

Manuscript received October 5, 2020; revised November 24, 2020; accepted December 14, 2020. Date of publication December 23, 2020; date of current version February 22, 2021. This article was recommended for publication by Associate Editor M. Munih and Editor P. Dario upon evaluation of the reviewers' comments. This work was supported by the National Research Foundation of Korea (NRF) Grant funded by the Korean Government (MSIT) under Grant NRF2016R1A5A1938472. The work of Sudeok Kim and Jooeun Ahn is supported by the Institute of Sport Science, Seoul National University, Seoul, Republic of Korea *(Corresponding authors: Kyu-Jin Cho; Jooeun Ahn.)*

Sangheui Cheon, Brian Byunghyun Kang, Jongeun Lee, and Kyu-Jin Cho are with the Biorobotics Laboratory, Department of Mechanical Engineering, Seoul National University, Seoul 08826, South Korea, and also with the Soft Robotics Research Center, Seoul National University, Seoul 08826, South Korea (e-mail: sang.h.cheon@snu.ac.kr; kjcho@snu.ac.kr).

Daekyum Kim and Sungho Jo are with the Neuro-Machine Augmented Intelligence Laboratory, School of Computing, KAIST, Daejeon 34141, South Korea, and also with the Soft Robotics Research Center, Seoul National University, Seoul 08826, South Korea.

Sudeok Kim and Jooeun Ahn are with the Sports Engineering Laboratory, Department of Physical Education, Seoul National University, Seoul 08826, South Korea, also with the Soft Robotics Research Center, Seoul National University, Seoul 08826, South Korea, and also with the Institute of Sport Science, Seoul National University, Seoul 08826, South Korea (e-mail: ahnjooeun@snu.ac.kr).

HyunSik Gong is with the Department of Orthopedic Surgery, Seoul National University Bundang Hospital, Seoul National University College of Medicine, Seongnam 13620, South Korea.

This article has supplementary downloadable material available at https://doi.org/10.1109/TMRB.2020.3046847, provided by the authors.

Digital Object Identifier 10.1109/TMRB.2020.3046847

I. Introduction

INTENTIONS of human actions are reflected in biological signals. A human muscle is composed of multiple motor units, and surface electromyography (EMG) records the generation and propagation of muscle unit action potentials (MUAPs) from the surface of the skin [1]. By monitoring MUAPs, a myoelectric interface based on EMG provides a communication window that transfers human movement intentions into control commands for prosthetics [2]–[4], exoskeletons [5]–[8], or robotic manipulators [9].

For the past few decades, myoelectric interfaces with EMG sensors fueled hope in enabling intuitive human–exoskeleton co-operation. Still, there are few practical issues to solve before implementing myoelectric interfaces into robotic gloves that augment human motor performance.

One major issue is the requirement of multiple EMG sensors for hand-related intention interpretation [10], [11]. To date, EMG sensors were usually placed between the muscle innervation zones and tendon zones because these regions were known to provide the best signal quality [12] (we will use the term 'muscle mid-lines' for these locations). However, human forearms are composed of multiple overlapping muscles that hide the muscle mid-lines from the surface of the skin, which hinders the EMG sensors from accessing clear myoelectric signals [13]. For example, the flexor digitorum superficialis (FDS), a finger flexor muscle, is overlapped by the flexor carpi-radialis (FCR) and ulnaris (FCU), the wrist flexor muscles, and this anatomical feature hampers accessing the myoelectric signals from the FDS only [13], [14]. Therefore, it has been necessary to utilize pattern analysis technologies with multiple sensors to overcome signal interference from synergistic muscle activations or crosstalks [15]. In addition, a process for placing the sensors requires a procedure of finding the optimal locations, which differ from person to person due to anthropometric differences among individuals. Designing a functional myoelectric interface necessitates this cumbersome process of customization, and the necessary effort obviously increases with the number of sensors.

Another critical issue is that myoelectric interfaces on the forearm usually do not guarantee reliability in actual situations where humans interact with the surrounding environment. Human actions for handling objects mostly involve changes in the arm posture, and these changes have detrimental effects on the pattern recognition performance of the interface [16], [17].

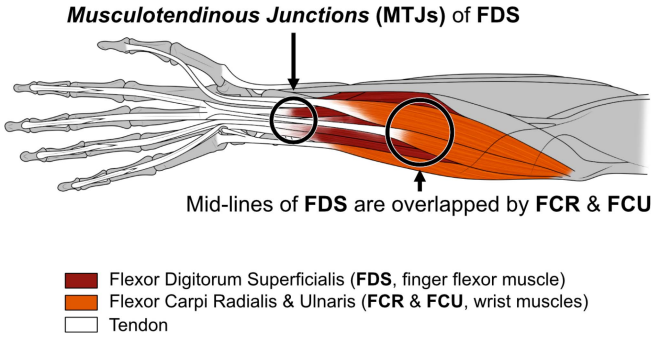

Fig. 1. Location of the *musculotendinous junctions* (MTJs) of the flexor digitorum superficialis (FDS). Since wrist related muscles do not overlap the MTJs of the FDS, the myoelectric signals from the MTJs interfere less with other signals from wrist muscles, compared to other signals from the muscle mid-lines in the forearm.

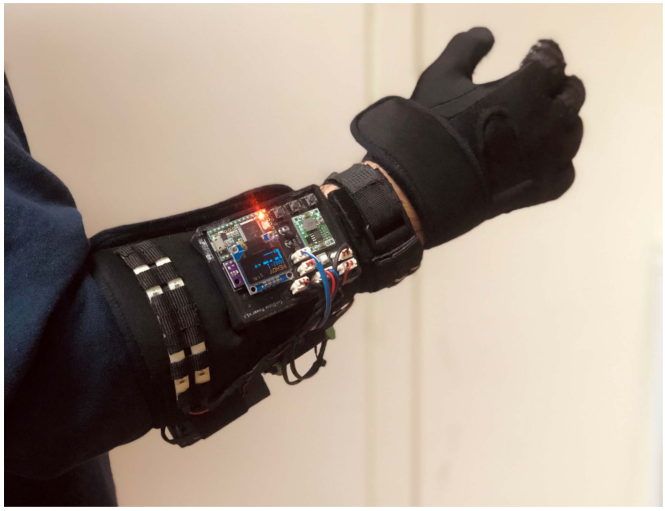

Fig. 2. System overview. Exo-Glove Power (EGPO) is a compact/portable soft robotic glove for augmenting the grasping force while the user intends a firm power grasp to secure an object. The single EMG sensor-based myoelectric interface in EGPO identifies the user's power grasp intention to actuate the robot.

The locations of muscle innervation zones shift when human joints rotate, and this can change the properties of myoelectric signals from the muscle mid-lines [18]. Moreover, various and even unanticipated patterns of human movements are usually introduced during actual operations [19]. Thus, to prevent any unintended operations of robotic gloves, the myoelectric interface has to distinguish the intended motion from other movements regardless of the arm posture changes.

The risk of an unexpected or improper operation becomes a particularly crucial issue when exoskeletons transmit high-force to augment human motor performance. For example, a robotic glove that augments power grasps, which is frequently executed to handle power tools securely or lift heavy objects [20], directly co-operates with the user's fingers. In this situation, unintended actuation forces to the fingers could directly jeopardize the user's safety, which can be fatal in harsh environments. As an example of occupational cases, firefighters who need to grip and pull a firehose or lift heavy objects in disaster scenes need to maintain high grip strength [21]. For manipulating objects in outer space, astronauts as well need high grip strength to compensate for the deterioration in grasp performance when using extravehicular gloves [22]. For such occupations, guaranteed safety is critical in the development of robotic gloves that augment power grasping. Myoelectric interfaces for such hand exoskeletons should robustly identify the power grasp intention from other intended motions such as wrist movements, even at the maximum voluntary contraction (MVC) level, regardless of arm posture changes. For example, the robotic glove should not augment grasping during wrist movements.

In this study, we show that a myoelectric interface on the *musculotendinous junctions* (MTJs) of the FDS enables reliable control of a robotic glove with a single EMG sensor by identifying power grasp intentions. The MTJs were known to provide low-quality myoelectric signals. However, we found that the EMG signals from the MTJs of the FDS (Fig. 1) show significantly increased amplitudes exclusively when a high-force power grasp is performed. Since wrist related muscles do not overlap the MTJs of the FDS, the myoelectric signals from the MTJs interfere less with other signals from wrist muscles, compared to other signals from the muscle mid-lines in the forearm [23]. Furthermore, these characteristics did not alter significantly across arm posture changes tested in this study. We utilized this feature to develop a myoelectric interface for a robotic glove that augments the user's power grasping force. By designing the interface to react only to high amplitude myoelectric signals of the MTJs, human movement patterns other than high-force power grasping, such as a delicate manipulation or wrist flexion up to the MVC level, can be rejected. This property enables reliable control of a hand exoskeleton. Here, we quantitatively demonstrated that sensing myoelectric signals from a single sensor on the MTJs has clear advantages over using multiple sensors around the proximal forearm when identifying power grasp intentions. Exploiting the observed unique feature of the MTJs, we further propose two myoelectric control methods—Dual-threshold control (DTC) and Morse-code control (MCC)—for the myoelectric interface in a robotic glove, Exo-Glove Power (EGPO; Fig. 2). DTC enables direct co-operation between the user and the robot, even under muscle fatigue. MCC allows the user to send various commands to the device by means of distinct sequences of binary inputs of power grasps.

II. Experimental Evaluation

The objective of this section is to evaluate the performance of identifying power grasp intentions with a single sensor on the MTJs of the FDS (Fig. 1). The study was approved by the Seoul National University Institutional Review Board (IRB No. 1903/001-002, 1911/003-020). All experiments were conducted by following the approved protocol.

A. Methods for Myoelectric Data Acquisition

1) The Location of the MTJs: A medical doctor created a protocol for identifying the location of the MTJs of the FDS. According to the protocol, we palpated the volar side of the distal forearm to find the proximal margin of the rope-like,

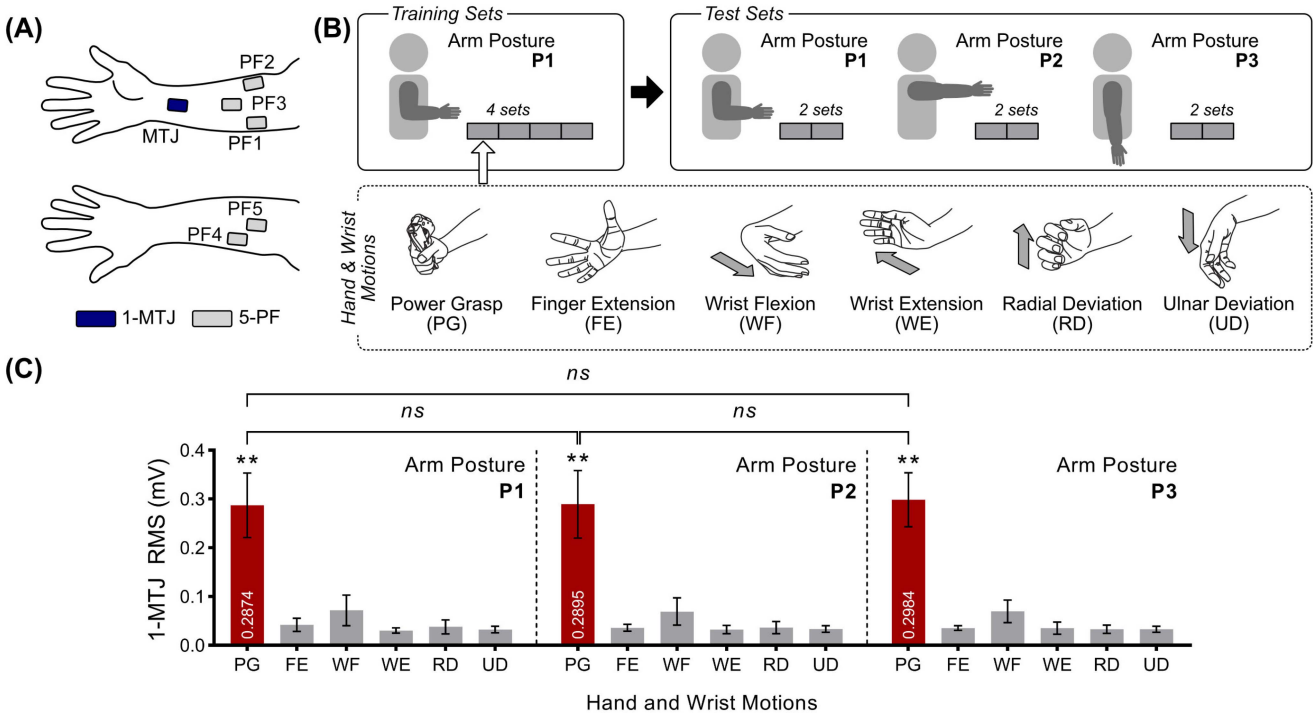

Fig. 3. Experimental design and preliminary evaluation. (A) Sensor locations. The classifiers were trained with the myoelectric signals from (i) one sensor on the MTJs of the FDS (1-MTJ) and (ii) five sensors around the proximal forearm (5-PF). (B) Three arm postures and six hand/wrist motions. Four sets from arm posture P1 were used to train the classifier, and two sets from each arm posture P1, P2, and P3 were used to test the classifier. All the motions were performed at the MVC level. (C) RMS values of the EMG signals from the MTJs of the FDS across all eight participants ($n = 8$, mean $\pm$ SD, total 80 sets). Bars are means, error bars denote SDs, *ns* denotes no statistical significance, and double asterisks denote statistical significance ($P < 0.01$).

multiple tendinous structures, which ranged typically between 4–8 cm from the wrist crease. The area around this margin was defined as the MTJs of the FDS in this study (Fig. 1).

2) Experiment Design: Eight healthy subjects ($n = 8$; five males and three females; age, 24.9 $\pm$ 0.6 y, mean $\pm$ SD) participated in the experiment. Six EMG sensors (Trigno Avanti, Delsys, USA) were attached to the forearm muscles targeting the following: (i) MTJs of the FDS, (ii) mid-lines of the flexor digitorum profundus and flexor carpi ulnaris, (iii) mid-line of the brachioradialis, (iv) mid-lines of the FDS and flexor carpi radialis, (v) mid-lines of the extensor carpi radialis brevis and extensor carpi radialis longus, and (vi) mid-line of the extensor digitorum (Fig. 3A). Each participant was asked to maintain six different motions—finger extension, power grasp, wrist extension, wrist flexion, ulnar deviation, and radial deviation—at the MVC level for 3 s (Fig. 3B). Participants used a hand gripper when performing power grasps. During the wrist motions, we instructed the participants not to make a fist to prevent unintended power grasping. An external structure was used to constrain the wrist to let the participants perform the wrist motions at the MVC level. Participants were asked to perform the tasks under three different arm postures—humerus hanging at the side, forearm horizontal (P1), straight arm reaching forward (P2), and straight arm reaching downward (P3). We collected six, two, and two sets of motion data for P1, P2, and P3, respectively, (Fig. 3B). The orders of both the postures and motions were randomized. The rest phases between each motion and each set were 3 and 10 min, respectively.

3) Signal Processing: The EMG signals were sampled at a frequency of 1,000 Hz. The data was filtered using a fourth-order Butterworth filter between 20 and 450 Hz to remove motion artifacts and high-frequency noise [24]. The motions were defined as 'intended' when the EMG signals from any of the six sensors were outside the double of the SD ranges of the relaxed muscle signals [24]. The mean absolute values (MAV), zero crossings (ZC), waveform lengths (WL), and slope sign changes (SSC) were calculated from the pre-processed EMG data with a window length of 250 ms and a step time of 50 ms (equation provided in the Appendix) [25]–[27].

B. Preliminary Evaluation

The root mean square (RMS) of the EMG data during six hand/wrist motions across three arm postures are presented in Fig. 3C. The RMS values of the signals from the MTJs during power grasping at the MVC level were 0.2874 $\pm$ 0.0661 mV for arm posture P1, 0.2895 $\pm$ 0.0692 mV for P2, and 0.2984 $\pm$ 0.0553 mV for P3 ($n = 8$, mean $\pm$ SD, total 80 sets). We observed that the RMS values of power grasping show statistically significant differences from those of other motions (unpaired t test, $P < 0.01$). This result clearly shows that the myoelectric signal amplitude (from the MTJs) jumps only when a power grasp is intended, and the tendency is maintained during arm posture changes. Based on the observation, we evaluated the performance of intention classification with the myoelectric signals from the MTJs.

TABLE I
HYPERPARAMETER SETTINGS TO TRAIN SVM

Notation	Description	Hyperparameter value
kernel	Kernel type	'poly'
degree	Polynomial degree	3
gamma	Kernel coefficient	10
C	Regularization parameter	1.0

C. Methods for Identifying Power Grasp Intentions

1) Classifier Design: Two support vector machine (SVM) classifiers were trained to distinguish the power grasp intention from other intended motions. One classifier was trained with the signals only from the MTJs of the FDS (1-MTJ), and the other classifier used signals from five sensors on the proximal forearm (5-PF). The features extracted for training the SVM classifier were the MAV, ZC, WL, and SSC [25]–[28]. The features were extracted from a 250 ms temporal window with a step time of 50 ms. To train the SVM classifier, Scikit-learn (a Python library for machine learning and data analysis) was used. In the library, the svm.SVC function was used for classifying grasping and non-grasping intention labels. Four datasets from arm posture P1 were used as training datasets. The training data was fed into the SVM classifier after being normalized by the min–max scaling, and the trained model was used to evaluate the test datasets composed of two sets from each of the three different arm postures (P1, P2, and P3). Detailed parameter settings are listed in Table I.

2) Metrics for Evaluation: Sensitivity and specificity were used for evaluating the identification performance, which are statistical measurements of binary classification performance [29]. To quantify sensitivity, we defined the true positive rate for grasping (TPRG), indicating how well the system detects true grasping activations. To quantify specificity, we defined the true negative rate for grasping (TNRG), indicating how well the system rejects false grasping activations. TPRG and TNRG are calculated as follows:

$$TPRG = P\left(pred_{grasping} \mid true_{grasping}\right) \quad (1)$$

$$TNRG = P\left(pred_{non-grasping} \mid true_{non-grasping}\right) \quad (2)$$

where *pred* refers to the predicted intention label, and *true* is the ground truth intention label.

D. Results

1) TPRG—Detection of Power Grasp Intentions: The sensitivity of 1-MTJ was compared with that of 5-PF for three different arm postures. For the arm posture P1, TPRGs measured using 1-MTJ and 5-PF were 88.19 ± 2.06% and 88.37 ± 2.96%, respectively (mean ± SEM; Fig. 4). For P2, TPRGs by 1-MTJ and 5-PF were 82.63 ± 1.85% and 78.55 ± 9.77%, respectively, and for P3, TPRGs by 1-MTJ and 5-PF were 85.99 ± 2.88% and 79.56 ± 9.75%, respectively, (mean ± SEM; Fig. 4). For any of the three arm postures (P1, P2, and P3), TPRGs by 1-MTJ did not show a statistically significant difference with the TPRGs by 5-PF (paired t test, $P > 0.05$).

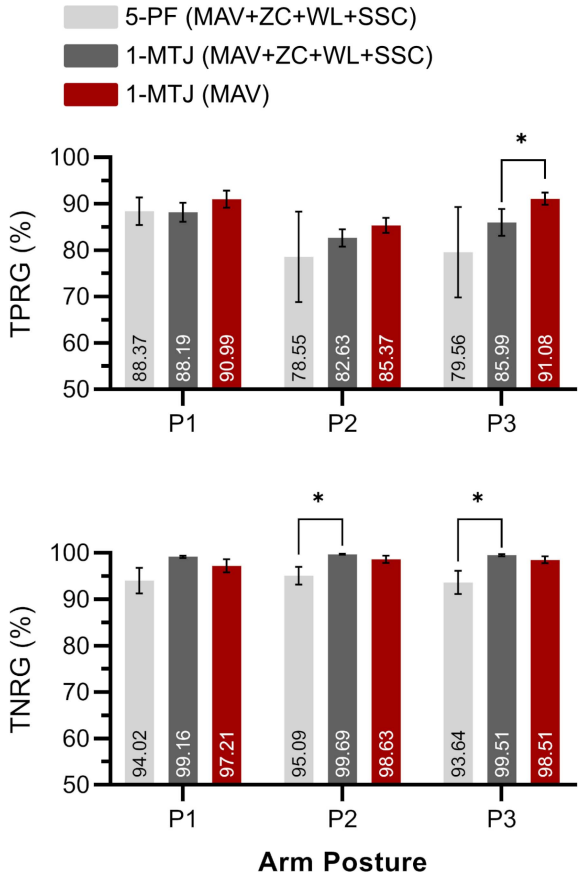

Fig. 4. Evaluation of the power grasp intention identification performance. Performance of the SVM classifiers; 5-PF used five sensors on the proximal forearm, and 1-MTJ used one sensor on the MTJs of the FDS. TPRG, true positive rate for grasping; TNRG, true negative rate for grasping. Bars are means, error bars represent SEMs, and asterisks denote statistical significance; $P < 0.05$.

2) TNRG—Rejection of Other Intentions: When using powered exoskeletons, prevention and rejection of unintended operations are the top priorities because any unintended operation of the robot could hinder the intended operation or injure the user [19]. The specificity of 1-MTJ was compared with that of 5-PF for the three arm postures. For the arm posture P1, TNRGs measured using 1-MTJ and 5-PF were 99.16 ± 0.26% and 94.02 ± 2.76%, respectively, which did not show a statistically significant difference (mean ± SEM; paired t test, $P = 0.1126$; Fig. 4). For P2, TNRGs by 1-MTJ and 5-PF were 99.69 ± 0.10% and 95.09 ± 1.89%, respectively, which showed statistically significant differences (mean ± SEM; paired t test, $P = 0.0477$; Fig. 4). For P3, TNRGs by 1-MTJ and 5-PF were 99.51 ± 0.26% and 93.64 ± 2.48%, respectively, which showed statistically significant differences (mean ± SEM; paired t test, $P = 0.0398$; Fig. 4).

In all three arm positions (P1, P2, P3) the means of TNRGs by 1-MTJ were higher than the means of TNRGs by 5-PF. In particular, when the arm posture changed from P1 to P2 or P3, the differences became statistically significant; 1-MTJ is better than 5-PF in rejecting movements other than power grasping under various arm postures. The observed higher specificity of 1-MTJ indicates that, in identifying power grasp intentions, a single sensor placed on the MTJs of the FDS performs more

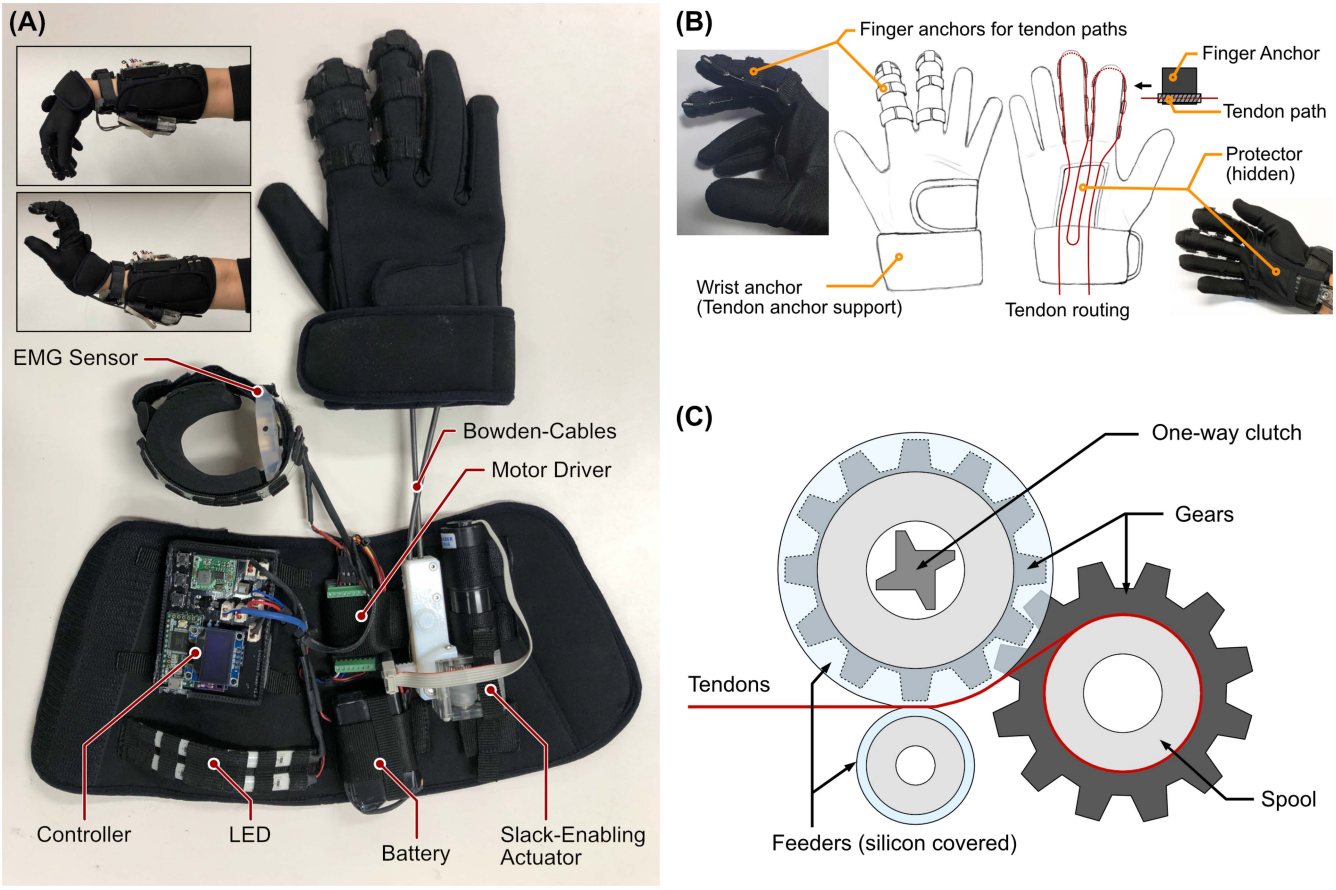

Fig. 5. System Design. (A) Hardware structure of Exo-Glove Power. The robotic glove does not restrict wrist motions. (B) Glove part structure. The differential mechanism from the tendon routing allowed the robotic glove to adapt when grasping objects of various shapes. (C) Structure of the slack-enabling actuator.

robustly than multiple sensors placed on the muscle mid-lines in actual activities involving changes in arm postures.

3) Feature Reduction: The characteristics of the myoelectric signals could differ from person to person and could also be affected by muscle conditions, such as muscle fatigue [30], [31]. One way to address these challenges is to reduce the number of extracted features and handle the characteristic change with proper methods. Since our initial approach was based on the myoelectric signal amplitude jumps during power grasps, we additionally trained an SVM classifier with the signals from the MTJs of the FDS using only one feature, the MAV. With this approach, TPRGs for arm posture P1, P2, and P3 became 90.99 $\pm$ 1.84%, 85.37 $\pm$ 1.62%, and 91.08 $\pm$ 1.32%, respectively, and TNRGs for arm posture P1, P2, and P3 became 97.21 $\pm$ 1.386%, 98.63 $\pm$ 0.78%, and 98.51 $\pm$ 0.72%, respectively (mean $\pm$ SEM; Fig. 4). The difference between the original performance of the 1-MTJ using all four features and the performance with this feature reduction was not statistically significant, except the TPRG for P3 ($P = 0.0458$).

Based on the result, we devised two single sensor-driven myoelectric control strategies that utilize only the MAVs of the myoelectric signals from the MTJs of the FDS, which is introduced in Section IV. The following section (Section III) explains the robotic glove into which we implemented the devised myoelectric control strategies.

III. System Design

A. Design of the Robotic Glove

A robotic glove, EGPO, with a myoelectric interface, was developed to demonstrate the devised myoelectric control methods. EGPO has a built-in EMG sensor (13-E200, Ottobock, Germany) that could be attached and fastened to the MTJs of the FDS. The hardware composition of EGPO is shown in Fig. 5. The tendon paths were reinforced with flexible metal components and anchored by webbing straps to enable high force transmission (Fig. 5B); the paths follow our previous robotic gloves developed for patients [32], [33]. The robot, including the actuator and battery, weighed 450 g (the glove only, 32 g), and was designed to fit inside an external protective glove. Users could freely move their wrists at the maximum range of motion while wearing the robotic glove (Fig. 5A).

B. Actuation Unit

A slack-enabling actuator was developed to prevent tendons around the spool from derailing when the tendons are not under tension. The previous version of the slack-enabling actuator was bulky due to its complicated structure and could not be mounted on the forearm [34]. To make EGPO portable, the spring-type jamming mechanism was replaced with feeders with a silicon cover (Fig. 5C). All the electrical components

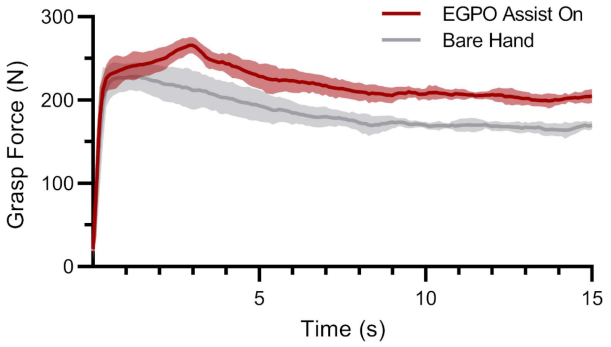

Fig. 6. Assistance profile of Exo-Glove Power (EGPO). The participant grasped a gripper with (i) the bare hand (gray) and (ii) EGPO (red) for ten trials each. During the 15 s of the experiment, EGPO provided 34.45 N of grasp force on average. The solid lines and error bands indicate the profiles of the means and SDs, respectively.

and the actuator (2232SR, Faulhaber, Switzerland) were placed on the forearm sleeve, close to the elbow, to reduce the effect of the inertia of the device on the arm movements.

C. Assistance Profile

To measure the assistive force provided by EGPO, experiments were performed on a single participant ($n = 1$; female; age, 26 y). The dimensions of the participant's hand were as follows: the index finger 84 mm, middle finger 95 mm (from the metacarpal joint to each fingertip), and the hand length 175 mm (from the tip of the middle finger to the base of the palm). A load cell (333FDX, Ktoyo, Korea) was enclosed in a 3D-printed gripper, and the length between the finger contact locations was 52 mm. The participant was asked to monitor the MAVs of EMG signals from the MTJs and maintain the MAVs while power grasping the gripper at the MVC level for 15 s. The participant performed ten sets of the aforementioned task, and each set comprised one trial with assistance from the robotic glove and one trial with the bare hand. Per each set, the order of the two trials was randomized. The rest phases between each trial and each set were 15 and 30 min, respectively. Five sets were performed on the first day of the experiment, and five additional sets were performed the next day. The force data was measured at a sampling frequency of 10 Hz. The wrist was kept in a neutral position in all trials. The results are presented in Fig. 6, and the mean assistive grasp force provided by the glove was 34.45 N (unpaired t test, $P < 0.001$).

IV. Single Sensor-Driven Myoelectric Control

A. Dual-Threshold Control

The role of EGPO is to assist the grasp force while the user intends a firm power grasp to secure an object (Supplementary Movie S1). A simple way to intuitively activate the robotic glove is to actuate the robot while the MAV exceeds a certain threshold. However, the forearm muscles fatigue fast during secure grasps [35], and the signal characteristics, including the MAV, can easily change as the user performs a long-durational power grasp. The increase in the MAVs will not deactivate the robot, but the decrease in the MAVs may deactivate the robot contrary to the user's intention. Therefore, we set a

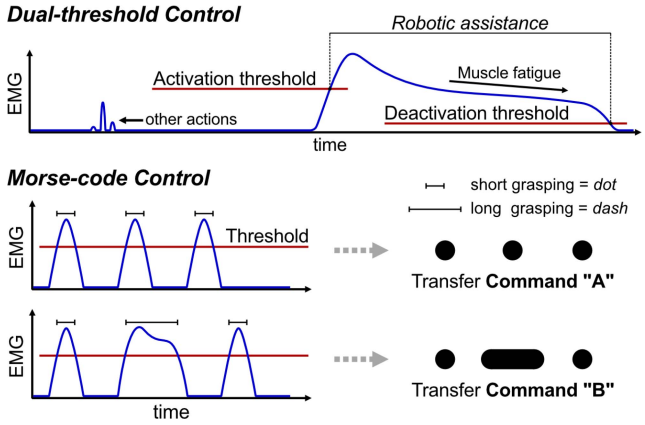

Fig. 7. Overview of the single sensor-driven myoelectric control strategies. Dual-threshold control (DTC) enables direct co-operation between the user and the robot, and Morse-code control (MCC) allows the user to send various commands to the device by means of distinct sequences of binary inputs of power grasps.

deactivation threshold separately from the activation threshold (Fig. 7). We implemented this control method in EGPO and validated its performance in practical operations that include a discrete/continuous grasping task (lifting a heavy bag, 15 kg) and a rhythmic/repetitive grasping task with dynamic arm movements (pulling a rope connected to a 15 kg bag).

1) Design of Dual-Threshold Control (DTC): Myoelectric signals were sampled at a rate of 500 Hz from the EMG sensor in EGPO (13-E200, Ottobock, Germany). The MAVs of the myoelectric signals were extracted from a 250 ms window with a step time of 200 ms using a microprocessor (Teensy 3.2, PJRC, USA). Two thresholds were set for activation and deactivation (Fig. 7). We determined these thresholds with two parameters: α and β. The activation threshold was set α % higher than the maximum MAVs of the signals when the other motions were performed at the full range or at the MVC level. In this study, we set α as 50. Increasing α will activate the robot at stronger grasping intentions. Note that the activation threshold should be set lower than the MVC level of power grasping. The deactivation threshold was set β % lower than the activation threshold to prevent unintended deactivation due to the gradual decrease in MAVs of the signal, e.g., by muscle fatigue. Here, we set β as 90. Lowering β will deactivate the robot faster when releasing is intended, but this will also make the robot less robust against muscle fatigue; the threshold values should be set according to the usage situation of the robotic glove. Therefore, EGPO was built with buttons to regulate the threshold values. When the MAVs of the signals exceeded the activation threshold or fell below the deactivation threshold, commands for motor control were transmitted to a motor driver (MCDC3002 S CO, Faulhaber, Switzerland). An OLED screen was used to display the MAV, robot status, and threshold values.

2) Human Subject Experiment I: The objective of this experiment was to monitor the performance of DTC in detecting the user's intention of power grasping in practical operations that include a discrete/continuous grasping task and a rhythmic/repetitive grasping task with dynamic arm movements. A single participant ($n = 1$; male; age, 38 y)

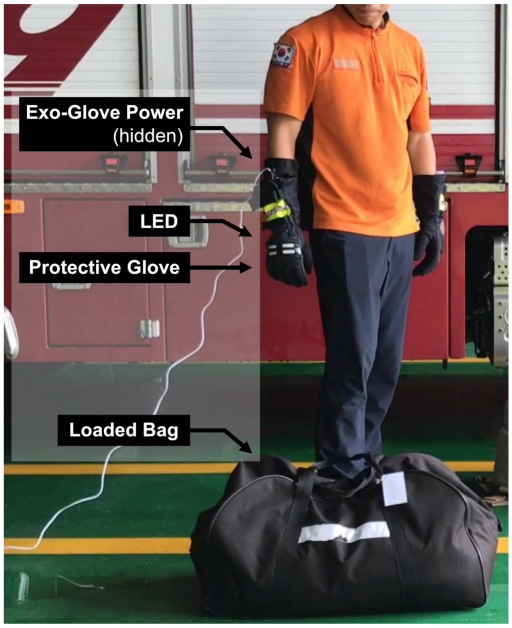

Fig. 8. Human subject testing of dual-threshold control. One healthy subject (n = 1; male fire fighter; age, 38 y) participated in this experiment. The participant was neither trained to use EGPO prior to the experiments nor instructed to perform a power grasp.

equipped with EGPO and a protective glove was asked to perform the aforementioned tasks (Fig. 8). An LED bar was attached to the outer side of the glove and lit while EGPO was activated. The participant was neither trained to use EGPO prior to the experiments nor instructed to perform a power grasp. A camcorder recorded the scene during the task. The participant activated EGPO by clenching his fist before conducting each task to synchronize the video recordings with the MAVs of the myoelectric signals. While performing each task, EMG data and robot activation levels were recorded. During 15 s of the continuous grasping task in which the participant should grasp and hold a heavy bag, the robot was activated for 98.89% of the period (Fig. 9A, Supplementary Movie S2). The robot was activated 170 ms after grasping and deactivated 130 ms after releasing. Between the initial grasping and releasing, the robot maintained actuation. While the participant repetitively pulled the rope for 10 s, the robot activated 152 $\pm$ 82 ms after grasping and deactivated 160 $\pm$ 71 ms after releasing (mean $\pm$ SD; Fig. 9B, Supplementary Movie S3). Twenty more trials of the repetitive grasping task are included in Supplementary Movie S3; EGPO was successfully activated for all grasping trials. This result shows that DTC is effective for dynamic arm movements as well as long-durational use.

3) Human Subject Experiment II: The objective of this experiment was to evaluate the robustness of DTC across multiple users. Three healthy subjects participated in this experiment (n = 3; two males and one female; age, 27 $\pm$ 0.67 y, mean $\pm$ SD). The participants fastened the myoelectric interface of EGPO themselves according to the protocol introduced in Section II-A1 and performed 10 sets of two motions, PG and WF, for 3 s at the MVC level with three different arm postures (P1, P2, and P3) in a randomized order. WF was selected as the representative motion other than PG because WF resulted in the highest MAV among 5 motions

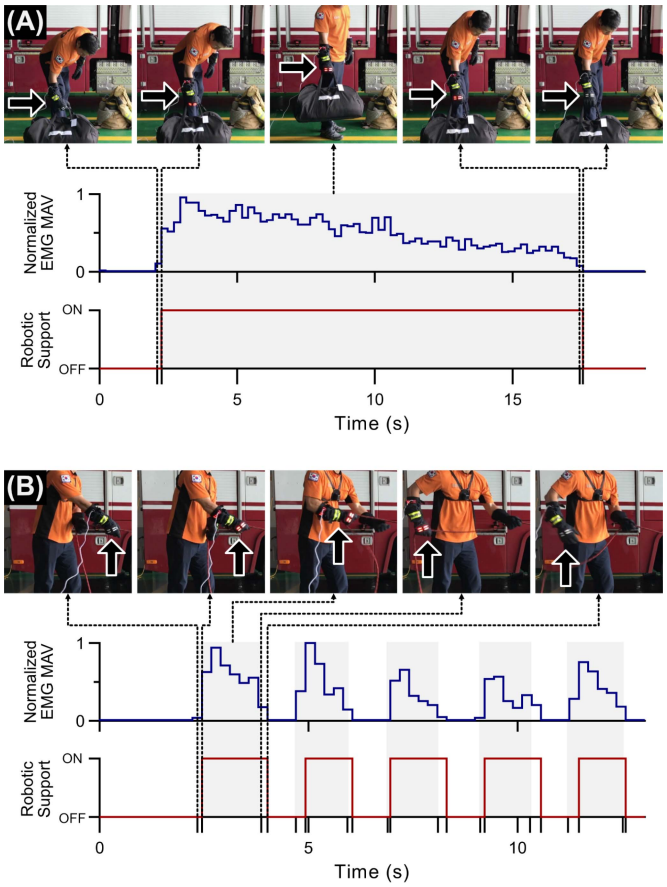

Fig. 9. Dual-threshold control during operations. (A) Continuous grasping. (B) Repetitive grasping. Gray shaded area indicate true grasping intentions.

TABLE II
ROBUSTNESS OF DUAL-THRESHOLD CONTROL

Participant	Activation counts[a]		EMG MAV (mean $\pm$ SD)[b]	
	PG	WF	PG	WF
S1	30	0	0.516 $\pm$ 0.032	0.064 $\pm$ 0.001
S2	30	0	0.352 $\pm$ 0.038	0.062 $\pm$ 0.001
S3	30	0	0.360 $\pm$ 0.034	0.044 $\pm$ 0.001

[a] Activated trials out of 30 trials for PG and WF, respectively.
[b] Normalized to the MVC level.

other than PG (Fig. 3C). We collected EMG data and checked whether EGPO was activated during each set. The results are tabulated in Table II; EGPO was activated for all PG trials and deactivated for all WF trials for all three participants and all three arm postures.

B. Morse-Code Control

The myoelectric interface with DTC can provide intuitive on/off binary control commands since it can reliably identify power grasp intentions. However, the users may often need to send various command options for efficient operations: a command to enter a 'permanent assist mode' to lift an object for a long time with no effort, a command for turning off the assist mode temporarily, or a command for activating other

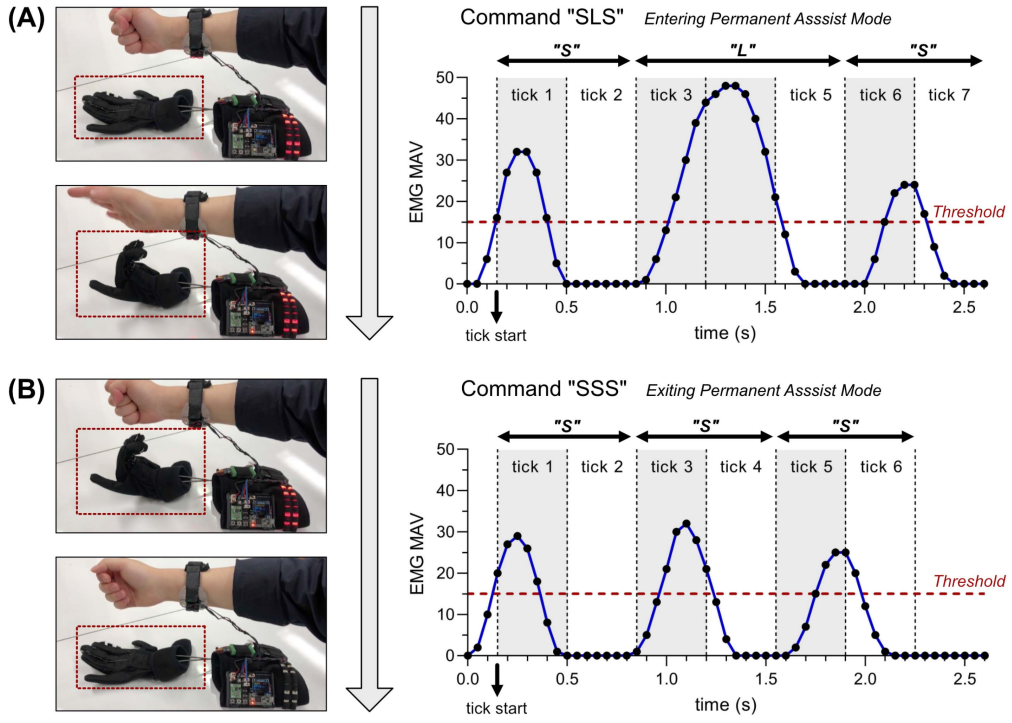

Fig. 10. Morse-code control. (A) Entering 'permanent assist mode' with command "SLS." EGPO maintains actuation although the user's hand is at rest. (B) Exiting 'permanent assist mode' with command "SSS." The full process is shown in Supplementary Movie S4. "S" stands for short grasping. "L" stands for long-durational grasping.

exoskeletons. To send multiple commands with a binary identifier, we used a control method inspired by *Morse code* (Fig. 7). By commanding with sequences of two different power grasp durations, which are dots and dashes in *Morse code*, users can send multiple commands with binary inputs. Performing a short grasp, which makes the MAV exceed a certain threshold for a short period of time, could act as a dot ("S" for short grasp), and a long holding grasp could act as a dash ("L" for long holding grasp).

1) Design of Morse-Code Control (MCC): The MAVs of the myoelectric signals were extracted from a 250 ms window with a step time of 50 ms. To actualize MCC in a myoelectric interface, a timer was set to classify "S" (for a dot) and "L" (for a dash) grasping inputs for each sequence. If the MAV of the myoelectric signal exceeds a certain threshold, the timer starts and monitors the MAV during each tick whose interval is 350 ms. If a short-durational power grasp is performed so that the MAV drops below the threshold before or during the second tick, this action will be classified as "S" (dot). Holding a long-durational power grasp, which makes the MAV drop below the threshold during the third tick, will be classified as "L" (dash) (Fig. 10). After collecting three sequences, the interface determines the command that the user intends.

The command to enter and exit 'permanent assist mode' was realized in EGPO by using three sequences of inputs. Each command requires a different level of effort in execution; the "SSS" command will be the easiest to execute, and the commands that combine "S" and "L" commands will be more effortful. However, the "SSS" command can be accidentally sent to the robot when the user does rhythmic/repetitive grasping quickly. Therefore, to avoid unintended operations, the sequence for initiating a specific mode should require some effort; we selected "SLS" for the commands to enter the permanent assist mode (Fig. 10A), and "SSS" to exit the mode (Fig. 10B).

2) Human Subject Experiment: The process of entering and exiting the 'permanent assist mode' is demonstrated in Fig. 10 and Supplementary Movie S4. The objective of the experiment was to evaluate the success rate (the number of successful executions out of the total number of trials) of MCC across multiple users, and six healthy subjects were recruited for this experiment ($n = 6$; four males and two females; age, 26.83 $\pm$ 0.90 y, mean $\pm$ SD). Each participant performed 20 trials for command "SSS" and "SLS", respectively, in a randomized order. The overall success rate was 91.67 $\pm$ 4.71% for command "SSS" and 73.33 $\pm$ 14.34% for command "SLS." The success rates of each participant are tabulated in Table III. For each of the "SSS" and "SLS" tasks, the total number of trials was 120 (six participants; 20 trials). Out of the 120 trials, the participants failed to command "SSS" and "SLS" in 10 and 32 trials, respectively. In all the 10 trials in which the participants failed to execute "SSS", the controller terminated the recognition process without misclassifying the users intention. In contrast, among the 32 trials in which the participants failed to execute "SLS", the controller classified the intended signals as "SSS" in 11 trials and terminated the recognition process in 21 trials.

V. Discussion

In this study, we exploited the unique anatomical feature of the MTJs and further devised two single-sensor based myoelectric control strategies for a robotic glove (Fig. 7).

TABLE III
SUCCESS RATE OF MORSE-CODE CONTROL

Participant	Success rate (%)	
	Command "SSS"	Command "SLS"
S1	90	80
S2	90	45
S3	85	80
S4	100	85
S5	95	65
S6	90	85
Total (mean ± SD)	91.67 ± 4.71	73.33 ± 14.34

The compactness and reliability of the control interface facilitate high wearability and safe operation, whose absence has long hampered the practical use of myoelectric interfaces in hand exoskeletons. We highlighted the effectiveness of the myoelectric interface by implementing it into a robotic glove and presenting its performance in practical operations. DTC enables direct co-operation between the user and the robot, and MCC provides various command options for the user.

Although robotic gloves can utilize force-sensors located on the fingertips to detect firm grasping intentions when augmenting grasp force [36], [37], unintended actuation can occur when fingers are in contact with an object without flexion, such as in the case of pushing heavy doors with open hands. Also, the electrical components on the glove's contact point have a risk of impairment when the user vigorously interacts with the object in a harsh environment. On the other hand, a grasp-related intention detection method based on the kinematics of the hand (e.g., bending sensors on the fingers) may be an alternative, but this method also has limitations for interpreting the force-levels of intended actions. Actions such as shaking hands or holding a pen require delicate and precise grasping, but an augmented grasp force in these situations could hinder the intended actions. These limitations are inevitable as long as the controller determines robotic actuation based only on the circumstantial information about the mechanical interaction between the user and an object, without considering the actual human intention. The proposed method circumvents these issues by removing all the electrical components from the glove and interpreting human intention from biological signals.

Unlike pattern recognition-based classifiers, the presented myoelectric control methods do not require multiple classifier training sets prior to the individual use of the robotic glove. Only a simple process of adjusting the threshold values for each user is required. Still, as shown in Section II, a pattern recognition-based classifier is an alternative method to DTC and has the potential for providing better performance, for example, by auto-calibrating the threshold parameters. In addition, since MCC decodes the patterns of grasping inputs with different duration, applying machine intelligence to MCC could provide higher accuracy in decoding intended commands.

We expect that reducing the number of required sensors to one can considerably facilitate the practical use of myoelectric interfaces in exoskeletons. Each human has different muscle sizes and configurations; therefore, locating EMG sensors on each individual's muscles requires a cumbersome process of customization. The development of a single sensor-based myoelectric interface substantially simplifies this process of location selection. However, the users are still required to locate a single sensor on the MTJs' ideal area, which is difficult to define precisely. Although the three participants in Section IV-A3 all succeeded in locating the EMG sensor on the functional area by following the protocol introduced in Section II-A1, better methods for finding the ideal electrode location might be developed in future studies to accelerate the practical use of the proposed system. For example, a computer vision-based automatic fitting system for the interface (or the whole robot) could be a potential solution for this limitation.

Before actually deploying the proposed system to end-users, several issues should be considered in prior. DTC theoretically rejects the effect of muscle fatigue, and we showed its performance with a single subject experiment. However, experiments with multiple human subjects and with a longer duration should be performed to examine the effects of muscle fatigue in DTC. Additionally, some participants showed a low success rate in executing command "SLS" for MCC (Table III; S2 and S5). We speculate that these participants struggled to keep the rhythmic timing of grasping inputs due to the lack of rhythm perception, the capacity to synchronize voluntary movements with the predicted future beats in a rhythmic sequence [38]. Whether a long-term practice and/or optimization of the static parameters can increase the decoding accuracy of MCC might be addressed in future studies.

There are also a few issues left in the aspect of using a myoelectric interface. We used commercial EMG sensors (Delsys and Ottobock) and did not evaluate the effects of the electrode size in the controller performance. Furthermore, the fastening structure for the EMG sensor should be improved for long-term use of the interface because any perturbed force on the current fastening structure could cause electrode shifts, which may deteriorate the controller performance.

In this study, we discovered one location over the MTJs, where the intention of generating a high grasp force could be robustly identified without being interfered by signals from other muscles. The MTJs of other muscles may also tentatively contribute to developing a compact and effective interface for exoskeletons and exosuits. For example, a runner's intention to sprint may be reliably detected by a sensor located on the MTJ of a major lower limb muscle.

APPENDIX
EQUATIONS FOR FEATURE EXTRACTION

The detailed guideline for feature extraction is introduced in Hudgins *et al.* [28].

A. Mean Absolute Value (MAV)

The MAV of signal x in the window was calculated as follows:

$$MAV = \frac{1}{N}\sum_{k=1}^{N}|x_k|$$

where N denotes the number of samples in the time window and x_k denotes the k^{th} sample.

B. Zero Crossing (ZC)

This feature is the number of times signal x crosses zero within the window. To avoid signal crossing counts due to low-level noise, a threshold was included. The ZC of signal x in the window was calculated as follows:

$$ZC = \frac{1}{N}\sum_{k=1}^{N-1} f_k,$$
$$f_k = \begin{cases} 1, \ x_k x_{k+1} < 0, \ |x_k - x_{k+1}| > x_{th} \\ 0, \ else \end{cases}$$

where N denotes the number of samples in the time window, x_k denotes the k^{th} sample, and x_{th} denotes the threshold. In this study, we set x_{th} as 0.015 V [27].

C. Waveform Length (WL)

This feature provides a measure of the complexity of signal x. It is defined as the cumulative length of the signal within the window. The WL of signal x in the window was calculated as follows:

$$WL = \frac{1}{N}\sum_{k=1}^{N-1}|x_{k+1} - x_k|$$

where N denotes the number of samples in the time window and x_k denotes the k^{th} sample.

D. Slope Sign Change (SSC)

This feature is related to signal frequency and is defined as the number of times the slopes of signal x change sign within the window. To avoid noise-induced counts, a count threshold was used. The SSC of signal x in the window was calculated as follows:

$$SSC = \frac{1}{N}\sum_{k=1}^{N-1} f_k,$$
$$f_k = \begin{cases} 1, \ \left[(x_k > x_{k-1}, x_k > x_{k+1}) \, or \, (x_k < x_{k-1}, x_k < x_{k+1})\right] \\ \quad and \ \left[(|x_k - x_{k-1}| > x_{th}) \, or \, (|x_k - x_{k+1}| > x_{th})\right] \\ 0, \ else \end{cases}$$

where N denotes the number of samples in the time window, x_k denotes the k^{th} sample, and x_{th} denotes the threshold. In this study, we set x_{th} as 0.015 V [27].

ACKNOWLEDGMENT

The authors thank J. J.-R. S. for assisting the graphical presentation of the figures. The authors also thank Gwanak Fire Station (Seoul, Korea) for participating in the experiments.

REFERENCES

[1] D. Farina, R. Merletti, and R. M. Enoka, "The extraction of neural strategies from the surface EMG," *J. Appl. Physiol.*, vol. 96, no. 4, pp. 1486–1495, 2004.
[2] J. M. Hahne, M. A. Schweisfurth, M. Koppe, and D. Farina, "Simultaneous control of multiple functions of bionic hand prostheses: Performance and robustness in end users," *Sci. Robot.*, vol. 3, no. 19, 2018, Art. no. eaat3630.
[3] A. Furui *et al.*, "A myoelectric prosthetic hand with muscle synergy–based motion determination and impedance model–based biomimetic control," *Sci. Robot.*, vol. 4, no. 31, 2019, Art. no. eaaw6339.
[4] N. Lan, C. M. Niu, M. Hao, C.-H. Chou, and C. Dai, "Achieving neural compatibility with human sensorimotor control in prosthetic and therapeutic devices," *IEEE Trans. Med. Robot. Bionics*, vol. 1, no. 3, pp. 122–134, Aug. 2019.
[5] K. O. Thielbar *et al.*, "Benefits of using a voice and emg-driven actuated glove to support occupational therapy for stroke survivors," *IEEE Trans. Neural Syst. Rehabil. Eng.*, vol. 25, no. 3, pp. 297–305, Mar. 2017.
[6] P. Polygerinos, Z. Wang, K. C. Galloway, R. J. Wood, and C. J. Walsh, "Soft robotic glove for combined assistance and at-home rehabilitation," *Robot. Auton. Syst.*, vol. 73, pp. 135–143, Nov. 2015.
[7] T. Bützer *et al.*, "Pexo-a pediatric whole hand exoskeleton for grasping assistance in task-oriented training," in *Proc. IEEE 16th Int. Conf. Rehabil. Robot. (ICORR)*, 2019, pp. 108–114.
[8] K. Gui, U.-X. Tan, H. Liu, and D. Zhang, "Electromyography-driven progressive assist-as-needed control for lower limb exoskeleton," *IEEE Trans. Med. Robot. Bionics*, vol. 2, no. 1, pp. 50–58, Feb. 2020.
[9] P. K. Artemiadis and K. J. Kyriakopoulos, "EMG-based control of a robot arm using low-dimensional embeddings," *IEEE Trans. Robot.*, vol. 26, no. 2, pp. 393–398, Apr. 2010.
[10] M. Hakonen, H. Piitulainen, and A. Visala, "Current state of digital signal processing in myoelectric interfaces and related applications," *Biomed. Signal Process. Control*, vol. 18, pp. 334–359, Apr. 2015.
[11] X. Zhang, X. Chen, Y. Li, V. Lantz, K. Wang, and J. Yang, "A framework for hand gesture recognition based on accelerometer and EMG sensors," *IEEE Trans. Syst., Man, Cybern. A, Syst. Humans*, vol. 41, no. 6, pp. 1064–1076, Nov. 2011.
[12] L. Mesin, R. Merletti, and A. Rainoldi, "Surface EMG: The issue of electrode location," *J. Electromyogr. Kinesiol.*, vol. 19, no. 5, pp. 719–726, 2009.
[13] M. B. I. Reaz, M. S. Hussain, and F. Mohd-Yasin, "Techniques of EMG signal analysis: Detection, processing, classification and applications," *Biol. Procedures Online*, vol. 8, no. 1, pp. 11–35, 2006.
[14] J. P. Mogk and P. J. Keir, "Crosstalk in surface electromyography of the proximal forearm during gripping tasks," *J. Electromyogr. Kinesiol.*, vol. 13, no. 1, pp. 63–71, 2003.
[15] M. A. Oskoei and H. Hu, "Myoelectric control systems—A survey," *Biomed. Signal Process. Control*, vol. 2, no. 4, pp. 275–294, 2007.
[16] A. Fougner, E. Scheme, A. D. Chan, K. Englehart, and Ø. Stavdahl, "Resolving the limb position effect in myoelectric pattern recognition," *IEEE Trans. Neural Syst. Rehabil. Eng.*, vol. 19, no. 6, pp. 644–651, Dec. 2011.
[17] H.-J. Hwang, J. M. Hahne, and K.-R. Müller, "Real-time robustness evaluation of regression based myoelectric control against arm position change and donning/doffing," *PLoS ONE*, vol. 12, no. 11, 2017, Art. no. e0186318.
[18] S. Martin and D. MacIsaac, "Innervation zone shift with changes in joint angle in the brachial biceps," *J. Electromyogr. Kinesiol.*, vol. 16, no. 2, pp. 144–148, 2006.
[19] A. De Santis, B. Siciliano, A. De Luca, and A. Bicchi, "An atlas of physical human–robot interaction," *Mech. Mach. Theory*, vol. 43, no. 3, pp. 253–270, 2008.
[20] M. R. Cutkosky, "On grasp choice, grasp models, and the design of hands for manufacturing tasks," *IEEE Trans. Robot. Autom.*, vol. 5, no. 3, pp. 269–279, Jun. 1989.
[21] *National Fire Protection Association*. Accessed: Mar. 18, 2019. [Online]. Available: www.nfpa.org
[22] A. Villoslada, C. Rivera, N. Escudero, F. Martin, D. Blanco, and L. Moreno, "Hand exo-muscular system for assisting astronauts during extravehicular activities," *Soft Robot.*, vol. 6, no. 1, pp. 21–37, 2019.
[23] C. A. Boles, S. Kannam, and A. B. Cardwell, "The forearm: Anatomy of muscle compartments and nerves," *Amer. J. Roentgenol.*, vol. 174, no. 1, pp. 151–159, 2000.
[24] P. Konrad, *The ABC of EMG: A Practical Introduction to Kinesiological Electromyography*, vol. 1, Noraxon INC., Scottsdale, AZ, USA, 2005, pp. 30–35.

[25] A. Phinyomark, F. Quaine, S. Charbonnier, C. Serviere, F. Tarpin-Bernard, and Y. Laurillau, "EMG feature evaluation for improving myoelectric pattern recognition robustness," *Expert Syst. Appl.*, vol. 40, no. 12, pp. 4832–4840, 2013.

[26] M. A. Oskoei and H. Hu, "Support vector machine-based classification scheme for myoelectric control applied to upper limb," *IEEE Trans. Biomed. Eng.*, vol. 55, no. 8, pp. 1956–1965, Aug. 2008.

[27] D. Tkach, H. Huang, and T. A. Kuiken, "Study of stability of time-domain features for electromyographic pattern recognition," *J. Neuroeng. Rehabil.*, vol. 7, no. 1, p. 21, 2010.

[28] B. Hudgins, P. Parker, and R. N. Scott, "A new strategy for multifunction myoelectric control," *IEEE Trans. Biomed. Eng.*, vol. 40, no. 1, pp. 82–94, Jan. 1993.

[29] D. G. Altman and J. M. Bland, "Diagnostic tests. 1: Sensitivity and specificity," *Brit. Med. J.*, vol. 308, no. 6943, p. 1552, 1994.

[30] J. H. Viitasalo and P. V. Komi, "Signal characteristics of EMG during fatigue," *Eur. J. Appl. Physiol. Occup. Physiol.*, vol. 37, no. 2, pp. 111–121, 1977.

[31] B. Bigland-Ritchie, R. Johansson, O. Lippold, and J. Woods, "Contractile speed and EMG changes during fatigue of sustained maximal voluntary contractions," *J. Neurophysiol.*, vol. 50, no. 1, pp. 313–324, 1983.

[32] H. In, B. B. Kang, M. Sin, and K.-J. Cho, "Exo-glove: A wearable robot for the hand with a soft tendon routing system," *IEEE Robot. Autom. Mag.*, vol. 22, no. 1, pp. 97–105, Mar. 2015.

[33] B. B. Kang, H. Choi, H. Lee, and K.-J. Cho, "Exo-glove poly II: A polymer-based soft wearable robot for the hand with a tendon-driven actuation system," *Soft Robot.*, vol. 6, no. 2, pp. 214–227, 2019.

[34] H. In, U. Jeong, H. Lee, and K.-J. Cho, "A novel slack-enabling tendon drive that improves efficiency, size, and safety in soft wearable robots," *IEEE/ASME Trans. Mechatronics*, vol. 22, no. 1, pp. 59–70, Feb. 2017.

[35] M. A. Johnson, J. Polgar, D. Weightman, and D. Appleton, "Data on the distribution of fibre types in thirty-six human muscles. An autopsy study," *J. Neurol. Sci.*, vol. 18, no. 1, pp. 111–129, 1973.

[36] M. Diftler *et al.*, "RoboGlove—A robonaut derived multipurpose assistive device," in *Proc. IEEE Int. Conf. Robot. Autom. (ICRA)*, 2014, pp. 78–84.

[37] M. Nilsson, J. Ingvast, J. Wikander, and H. von Holst, "The soft extra muscle system for improving the grasping capability in neurological rehabilitation," in *Proc. IEEE-EMBS Conf. Biomed. Eng. Sci.*, Langkawi, Malaysia, 2012, pp. 412–417.

[38] L.-A. Leow and J. A. Grahn, "Neural mechanisms of rhythm perception: Present findings and future directions," in *Neurobiology of Interval Timing*. New York, NY, USA: Springer, 2014, pp. 325–338.